Neuron, Vol. 31, 87–101, July 19, 2001, Copyright ©2001 by Cell Press

Multiple Phosphorylation of Rhodopsin and the In Vivo Chemistry Underlying Rod Photoreceptor Dark Adaptation

Matthew J. Kennedy,[1] Kimberly A. Lee,[1] Gregory A. Niemi,[1,3] Kimberley B. Craven,[2] Gregory G. Garwin,[4] John C. Saari,[1,4] and James B. Hurley[1,3,5]

[1] Department of Biochemistry
Box 357350
[2] Department of Physiology and Biophysics
Box 357290
[3] Howard Hughes Medical Institute
Box 357370
[4] Department of Ophthalmology
Box 356485
University of Washington
Seattle, Washington 98195

Summary

Dark adaptation requires timely deactivation of phototransduction and efficient regeneration of visual pigment. No previous study has directly compared the kinetics of dark adaptation with rates of the various chemical reactions that influence it. To accomplish this, we developed a novel rapid-quench/mass spectrometry-based method to establish the initial kinetics and site specificity of light-stimulated rhodopsin phosphorylation in mouse retinas. We also measured phosphorylation and dephosphorylation, regeneration of rhodopsin, and reduction of all-*trans* retinal all under identical in vivo conditions. Dark adaptation was monitored by electroretinography. We found that rhodopsin is multiply phosphorylated and then dephosphorylated in an ordered fashion following exposure to light. Initially during dark adaptation, transduction activity wanes as multiple phosphates accumulate. Thereafter, full recovery of photosensitivity coincides with regeneration and dephosphorylation of rhodopsin.

Introduction

Intense illumination that stimulates a saturating response in a photoreceptor also induces light adaptation, an adjustment of the biochemical state of the cell that enables it to detect further stimulation. When such intense illumination is terminated, dark adaptation restores sensitivity to the retina. The earliest steps of dark adaptation require quenching of photoactivated rhodopsin by phosphorylation and binding of arrestin (Chen et al., 1995; Xu et al., 1997). On a slower time scale, all-*trans* retinal generated from rhodopsin photolysis must be reisomerised to the 11-*cis* configuration by the visual cycle and then recombined with opsin to regenerate rhodopsin. Genetic changes that impair quenching of phototransduction or regeneration of rhodopsin cause retinal disease. For example, mutations in arrestin and rhodopsin kinase have been linked to Oguchi disease (Fuchs et al., 1995; Yamamoto et al., 1997), and mutations in 11-*cis* retinol dehydrogenase have been linked to fundus albipunctatis (Yamamoto et al., 1999).

The study described here was initiated to address two fundamental unresolved issues about the molecular basis of dark adaptation. The first concerns the sites and kinetics of rhodopsin phosphorylation. Previous in vitro studies detected multiple phosphorylation at three primary phosphorylation sites, Ser-343, Ser-338, and Ser-334, within the carboxy-terminal tail of rhodopsin (Figure 1A). Ser-343 was identified in those studies as the favored initial site of phosphorylation (Papac et al., 1993; Ohguro et al., 1993; McDowell et al., 1993). However, a more recent analysis challenged those findings by concluding that Ser-343 is not phosphorylated and that multiple phosphorylation does not occur in vivo (Ohguro et al., 1995). The second unresolved issue is the origin of transduction activity during dark adaptation. In darkness following intense illumination, photoreceptors behave as if they are responding to dim background illumination that gradually fades with time (Stiles and Crawford, 1932; Jones et al., 1996; Thomas and Lamb, 1999). Activity within the transduction cascade subsides slowly as this "equivalent background" fades. The molecular origin of equivalent background has been controversial. Some studies suggest opsin (Cornwall and Fain, 1994) is the source, whereas others implicate phosphorylated metarhodopsin II (Leibrock et al., 1998). The possibility that different sources contribute at different times during adaptation has also been suggested (Fain et al., 2001).

To resolve these issues, we used a combination of biochemical, physiological, and genetic methodology to examine the molecular events that occur during dark adaptation. We first developed a mass spectrometry-based method to quantitate phosphorylation at each of the sites on the rhodopsin C terminus. A novel "flash and quench" device was developed to resolve on a subsecond time scale the initial rates of phosphorylation in isolated intact retinas. In order to establish relationships between phosphorylation and dark adaptation, we also analyzed rhodopsin phosphorylation in vivo. The phosphorylation assays we developed reduce perturbations, secondary effects, and other uncertainties that can arise when in vitro or mutagenesis-based methods are used to evaluate phosphorylation. This enabled us to directly compare our in vivo measurements of rhodopsin phosphorylation with the initial steps of the visual cycle, with regeneration of rhodopsin and with the electrophysiological parameters of dark adaptation. All these parameters were measured under the same in vivo conditions. Our findings establish the rates of phosphorylation and dephosphorylation at each site on rhodopsin in vivo and they implicate two types of equivalent background sources within the photoreceptor that decay at different rates.

Finally, to evaluate the relationship between rhodopsin phosphorylation and rhodopsin regeneration, we applied our method to the analysis of a genetically manipulated mouse in which rhodopsin regeneration is impaired. Cellular retinaldehyde binding protein (CRALBP) is required

[5] Correspondence: jbhhh@u.washington.edu

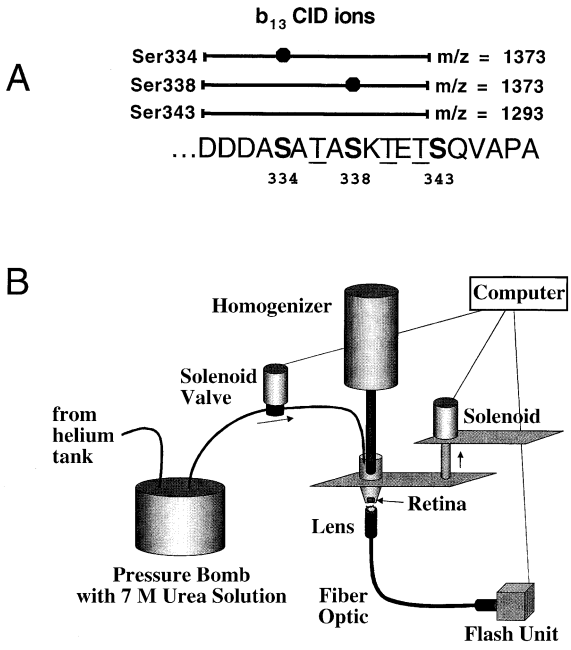

Figure 1. Analysis of Rhodopsin Phosphorylation

(A) Sequence of the mouse rhodopsin C terminus. The three serines that are the predominant sites of phosphorylation are in bold. Shown above the sequence are the CID fragments and their m/z values that were used to quantitate the relative amounts of Ser-343 and Ser-338 shown in Figure 2. The filled octagons represent phosphates.

(B) Rapid quench apparatus. The device is used as follows: freshly dissected mouse retinas in an oxygenated physiological solution are placed in the sample tube. Phosphorylation reactions are initiated by a flash from the strobe. At a specified time, a solenoid valve opens to allow pressurized 7 M urea to flow to the sample and a solenoid drives the sample tube up onto the tip of a homogenizer operating at maximum speed. Details are described in the Experimental Procedures section.

in vitro for efficient production of 11-*cis* retinol in the visual cycle (Winston and Rando, 1998; Stecher et al., 1999). Regeneration of rhodopsin is slowed nearly 15-fold in CRALBP-deficient mice (Saari et al., 2001). Using these mice, we found that phosphorylation and dephosphorylation of photolyzed rhodopsin occur independently of regeneration.

Results

Rhodopsin Phosphorylation within Seconds Following Illumination

Rapid kinetics of rhodopsin phosphorylation were analyzed using freshly dissected mouse retinas bathed at physiological temperature in an oxygenated physiological buffer. A novel type of rapid quench apparatus, described in Figure 1B, was developed to stop phosphorylation and dephosphorylation at times from 125 ms to 60 s after a bright flash. Following homogenization in 7 M urea, retinal membranes were washed and then digested with endo-proteinase Asp-N to release a C-terminal peptide of rhodopsin that encompasses all known phosphorylation sites (Figure 1A). The peptides were separated by reversed phase HPLC and detected and quantitated by electrospray ionization ion trap mass spectrometry. Elution profiles of unphosphorylated, singly, and multiply phosphorylated species in typical samples are shown in Figure 2A. Our method for detecting rhodopsin C-terminal peptides responded linearly within the range of 10 fmol to 100 pmol using synthetic unphosphorylated and monophosphosphorylated rhodopsin C-terminal peptides (data not shown). The sequence of these peptides was identical to that of the peptides we isolated from our biological samples.

The order of elution of various monophosphorylated peptides was established by analyzing collision-induced dissociation (CID) spectra of monophosphorylated (m/z = 973.3) peptides eluting from the column loaded with heavily phosphorylated samples. We confirmed the elution order using synthetic peptide standards monophosphorylated at each of the serines. CID fragments characteristic of peptides monophosphorylated on threonines were detected only at very low levels. The chromatography method we used separates rhodopsin C termini monophosphorylated at Ser-338 or Ser-343 from those phosphorylated at Ser-334 (Figure 2B). Peptides monophosphorylated at sites Ser-338 and Ser-343 eluted in overlapping peaks. Nevertheless, these peptides could be distinguished based on the characteristic CID fragments shown in Figure 1A. To calculate the relative amounts of Ser-338 and Ser-343 phosphorylated peptides, we integrated the m/z = 1373 and m/z = 1293 CID peaks as shown in Figure 2B. Efficiencies of detection of these fragment ions were determined using synthetic peptide standards. The validity of this method was confirmed by using it to calculate fractions of Ser-343 and Ser-338 peptides in mixtures of synthetic phosphorylated peptides of known composition (data not shown).

Figure 2C shows the time course of rhodopsin phosphorylation during the first 60 s following a brief flash of light that bleached ~40% of the rhodopsin in an isolated intact retina. Only monophosphorylated rhodopsin was formed initially, but seconds later, doubly and then triply phosphorylated species began to accumulate. Analyses of sites of phosphorylation are presented in Figure 2D, and the rates calculated from data during the first 5 s after the flash are presented in Table 1. Ser-343 was phosphorylated most rapidly and Ser-338 more slowly. Phosphorylation at Ser-334 begins after a delay of more than 10 s.

At 40% bleach, we expect that rhodopsin kinase operates near its V_{max}. The precise amount of rhodopsin kinase in a mouse rod has not been reported. However, based on the rate of phosphorylation at Ser-343 over the first few hundred milliseconds, and using a very rough estimate of ~1 rhodopsin kinase per 100–300 rhodopsins, each kinase could phosphorylate about one to three rhodopsin C termini per second in the steady state. It should be noted that the initial cycle of phosphorylation may occur rapidly, and the remaining steps required to reload the kinase with ATP could be slower. Therefore, the initial presteady-state rate of phosphorylation that would occur in response to a dim flash when the kinase is in excess over photoactivated rhodopsins could be significantly faster than the steady-state rate we report here.

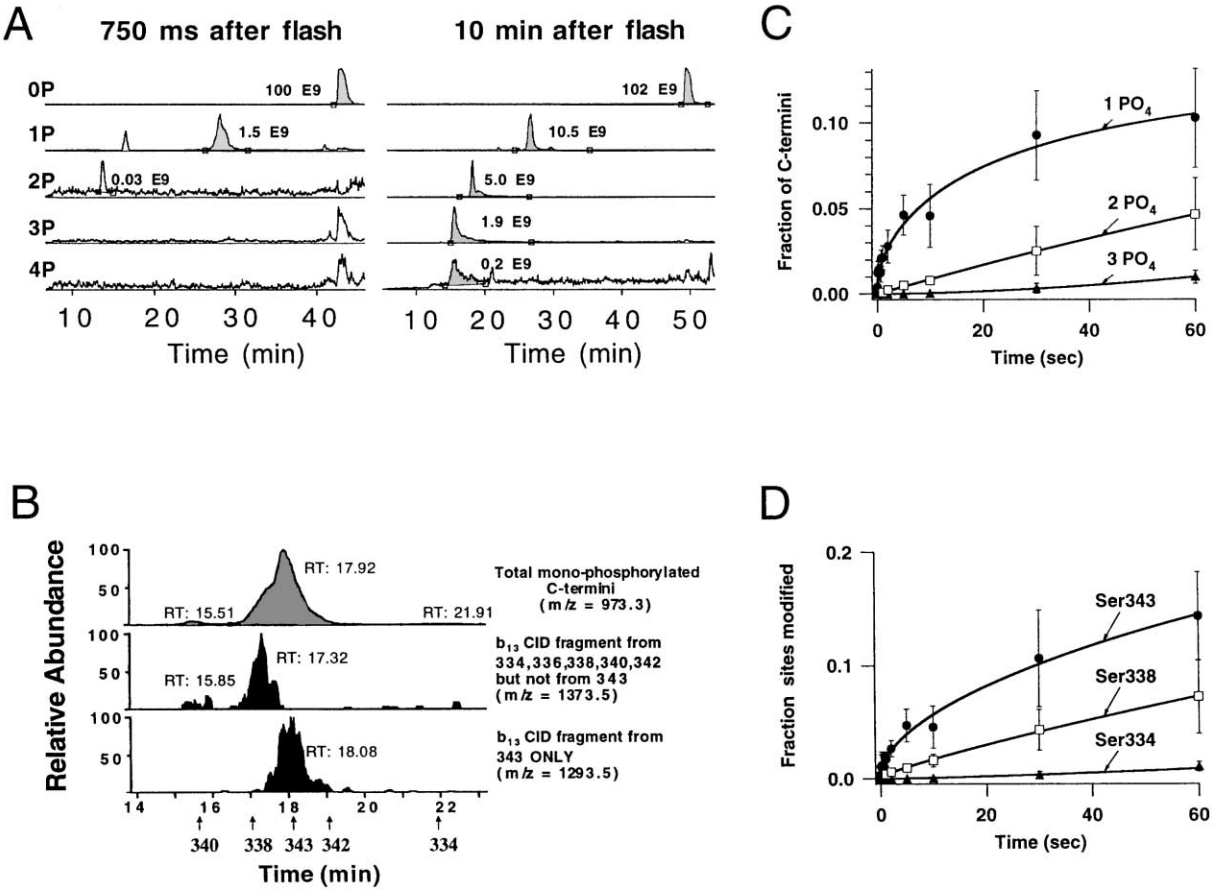

Figure 2. Method for Quantitating the Phosphorylation State of Rhodopsin and Early Time Course of Rhodopsin Phosphorylation

(A) HPLC elution profile of unphosphorylated (mass to charge ratio [m/z] = 933.3), singly phosphorylated (m/z = 973.3), doubly phosphorylated (m/z = 1013.3), triply phosphorylated (m/z = 1053.3), and quadruply phosphorylated (m/z = 1093.3) rhodopsin C-terminal peptides generated by proteolysis of retinal membranes with Asp-N proteinase as described in the Experimental Procedures section. Ions derived from C-terminal peptides were detected in their doubly charged state. The y axis in each panel represents the ion current normalized to the peak within the window of time shown. Only the shaded peaks were confirmed to be peptides derived from the rhodopsin C terminus. The numbers beside each shaded peak represent areas, e.g., "1.5E9" corresponds to 1.5×10^9 ions detected.

(B) Collision-induced dissociation (CID) spectra (ms-ms) of heavily phosphorylated samples and analyses of synthetic peptides established the order of elution of rhodopsin C termini monophosphorylated at different sites. Top panel: HPLC elution profile of total monophosphorylated C-terminal peptides from an early time point sample. The x axis represents elution time, and the y axis represents the abundance of ions eluting at a given retention time. Lower panels: CID (ms-ms) fragments were generated from the peptides eluting from the reverse phase column. Only ions with m/z = 973.3 ± 2.5 were selected for CID analysis. CID fragments were detected using mass to charge ratio (m/z) windows corresponding either to the b_{13} ion characteristic of a rhodopsin C-terminal peptide monophosphorylated at Ser-343 (m/z= 1293) or the b_{13} ion characteristic of all other monophosphorylated species (m/z = 1373). "RT" refers to the retention time on the reverse phase column.

(C) Kinetics of formation of singly, doubly, and triply phosphorylated rhodopsin from 0–60 s measured following a flash of light that bleached 40% of rhodopsin in dissected retinas. The y axis represents the fraction of total C termini detected. Error bars represent standard deviations in all figures.

(D) Kinetics of phosphorylation at Ser-343, Ser-338, and Ser-334. The y axis represents the fraction of all C-terminal peptides detected with a phosphate at the specified site. At these early times, nearly all of the doubly phosphorylated species are phosphorylated at Ser-343 and Ser-338. Phosphorylation at Ser-343 was estimated as the fraction monophosphorylated at Ser-343 plus the fraction of doubly and triply phosphorylated rhodopsin C termini. Phosphorylation of Ser-338 was estimated in the corresponding manner.

Measurements of Rhodopsin Phosphorylation and Dephosphorylation In Vivo

Phosphorylation of rhodopsin was also measured on a slower time scale using living mice exposed to flashes of white light. Mice were anaesthetized and exposed to a flash of light that bleached 20% of the rhodopsin in the eye. The measurements were done under experimental conditions identical to those used for the ERG measurements described in the next section. Mice were then sacrificed at various times from 30 s out to 5 hr following the flash, and whole eyes were homogenized directly in 7 M urea. Figure 3A shows the complete time course of rhodopsin phosphorylation and dephosphorylation under these conditions. An expanded view of the initial kinetics is also shown later in this report in Figure 6A. There was good agreement between the in vivo method and the rapid-quench method at 30 and 60 s.

Multiply phosphorylated opsins accumulated in vivo

Table 1. Kinetics of Phosphorylation[a]/Dephosphorylation[b] at Each Serine on Rhodopsin's C Terminus

	Rate of Phosphorylation[a]	Rate of Dephosphorylation[b]
Ser-343	2.6/min	0.14/min
Ser-338	0.48/min	0.074/min
Ser-334	0/min; 0.05/min	0.013/min

[a] Initial rate of phosphorylation during the first 5 s after the flash. Represented as the fraction of peptides phosphorylated at the specified site in the pool of photolyzed rhodopsin. The second value for Ser-334 is the rate between 1 and 3 min after the conditioning flash.
[b] Rate constants for dephosphorylation of Ser-343 and Ser-338 were derived from single exponential fits starting at the maximum level of phosphorylation for each particular site. For Ser-334, the fit was biphasic. Only the data points after 30 min were used for determination of the rate constant.

until 10–15 min after the conditioning flash. Subsequently dephosphorylation prevailed. Rates of dephosphorylation at each serine on rhodopsin's C terminus are shown in Figure 3B. The phosphatase acting on rhodopsin dephosphorylated Ser-343 slightly faster than Ser-338 and Ser-334 was dephosphorylated much more slowly (Table 1).

Since Ser-334 was dephosphorylated slowly, most of the monophosphorylated peptides we detected at later stages of dark adaptation were modified at Ser-334 (Figure 3B). This distribution was strikingly different from the distribution at earlier times when nearly all monophosphorylated peptides were modified at Ser-343 (Figure 2D). Analysis of a sample monophosphorylated primarily at Ser-334 is shown in Figure 4A. Approximately 40% of rhodopsin C-terminal peptides were monophosphorylated in this normal mouse sample that was taken 50 min after full bleach (see Figure 7). The lower two panels of Figure 4A show a comparison of elution profiles of peptides producing y_{11} CID ions with m/z = 1118.5 characteristic of Ser-334 phosphorylation versus peptides that produce the corresponding ions with m/z = 1198.5 characteristic of modification at other sites. Ser-334 modified peptides made up 80% of the monophosphorylated species in this sample. Analyses of monophosphorylated peptides from the 20% bleach experiments at 30–55 min were similar. However, the weaker CID signals specific for peptides phosphorylated at Ser-334 in those samples were noisier, and the shapes of the elution profiles were less clear.

We also analyzed sites of double phosphorylation during dark adaptation. Our model (presented later in this report; see Figure 8A) for opsin phosphorylation/dephosphorylation predicts that most doubly phosphorylated opsins would be modified at Ser-343 and Ser-338 at early times and at Ser-334 and Ser-338 at later times. We identified several ions produced by CID of these species and monitored their production from 20% bleach samples taken at early and late times during dark

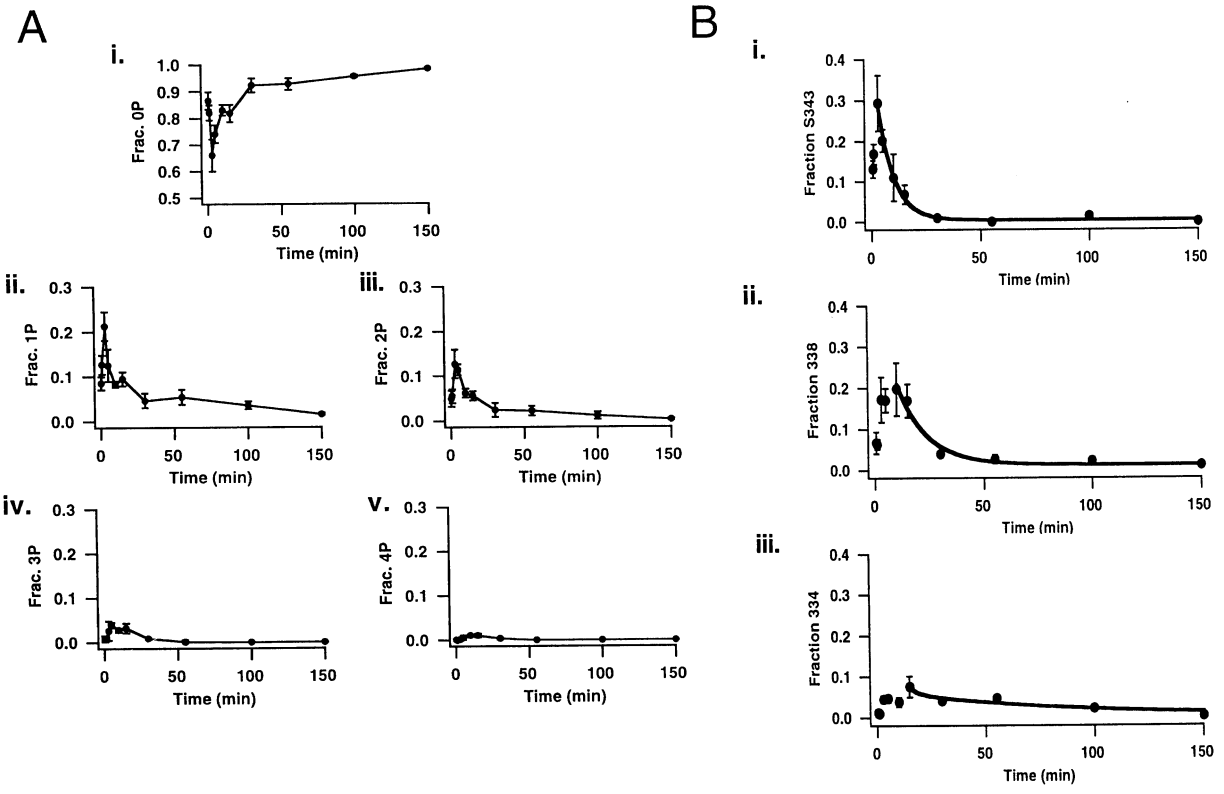

Figure 3. Time Course of Rhodopsin Phosphorylation and Dephosphorylation In Vivo Following a 20% Bleach

(A) Phosphorylation states: i. unphosphorylated, ii. monophosphorylated, iii. doubly phosphorylated, iv. triply phosphorylated, v. quadruply phosphorylated rhodopsin C termini.

(B) Dephosphorylation at specific sites. The solid lines are best fit single exponentials used to estimate dephosphorylation rates beginning at the maximum level of phosphorylation except for the Ser-334 data that was fit as a double exponential. i. Ser-343, ii. Ser-338, iii. Ser-334.

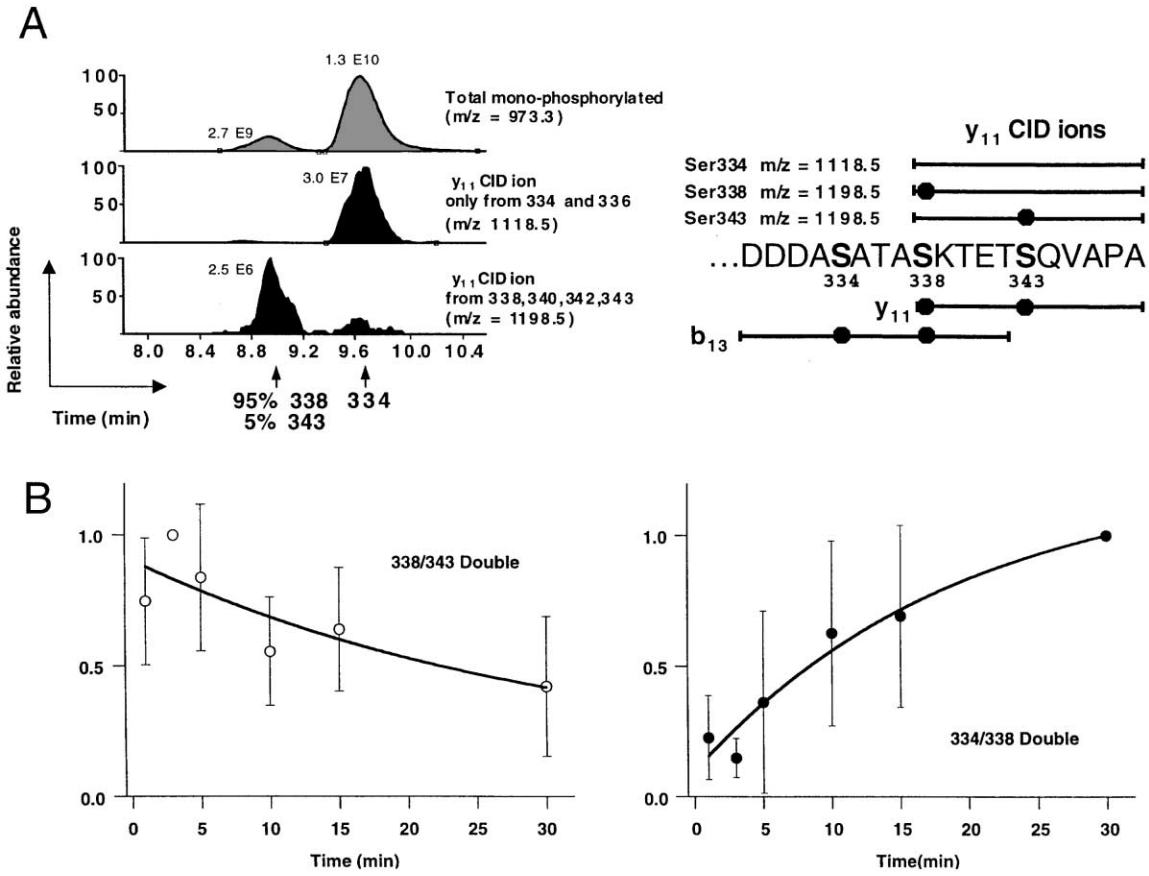

Figure 4. Identification of Monophosphorylated and Doubly Phosphorylated Opsin Species Following Photobleaching

(A) HPLC/mass spectrometry/CID analysis of a sample that consists primarily of Ser-334 modified peptides. The sample was taken from a wild-type mouse used in the experiment shown in Figure 7 50 min after a full bleach. 80% of the monophosporylated peptides were modified at Ser-334 in this sample. The panel on the right shows the origin of the CID fragments using the same conventions that were used in Figure 1A.

(B) Time course of the distribution of doubly phosphorylated species following a 20% bleach. Doubly phosphorylated peptides were analyzed by semiquantitative ms-ms analysis. The following CID fragments derived only from 334/338 doubly phosphorylated peptides were quantitated: m/z = 994.2 (b_9), 1122.3 (b_{10}), 1223.4 (b_{11}), 1352.4 (b_{12}), and 1453.5 (b_{13}). Ions that were derived only from 338/343 doubly phosphorylated peptides were also quantitated: 575.2 (b_6), 747.3 (b_8), and 1278.5 (y_{11}). There are no ions unique to 334/343 modified peptides. Each measurement was normalized to the yields of two CID ions produced from all species of doubly phosphorylated peptides, 1668.6 (b_{15}), and 1767.6 (b_{16}). The averaged data at each time point were then normalized to the maximum. The y axis therefore represents the relative fraction of all doubly phosphorylated opsins modified at 338/343 (left panel) or 334/338 (right panel) each normalized to its maximum time point. Although absolute levels could not be determined by this method, the decrease in 338/343 double phosphorylation during dark adaptation and the increase in 334/338 predicted by the model in Figure 8A are clearly demonstrated. The error bars represent the standard deviation.

adaptation. The results shown in Figure 4B confirmed our prediction by showing that CID fragments derived from Ser-338/Ser-343 phosphorylated opsins were produced most abundantly from samples taken at early times and fragments from Ser-334/Ser-338 were most abundant from samples taken at later times after the conditioning flash.

ERG Measurements of Dark Adaptation Parameters

We used ERG a-wave analysis to correlate our biochemical results with the physiology of dark adaptation. Parameters of dark adaptation were determined by recording ERG responses elicited by dim to moderate intensity test flashes given at various times following a single intense conditioning flash. The conditioning flash, anaesthetization, and illumination geometry were the same as those used for in vivo phosphorylation measurements. The leading edges of the a-waves were fit as an ensemble to a mathematical model of phototransduction (Breton et al., 1994) corrected for photoreceptor capacitance (Smith and Lamb, 1997) to calculate the parameters a_{max} and A. a_{max} is proportional to the fraction of channels open at the time of the test flash. Recovery of a_{max} during dark adaptation therefore corresponds to phototransduction turnoff. The parameter A represents how efficiently photoactivation of rhodopsin stimulates phototransduction. Recovery of A represents restoration of photoreceptor sensitivity during dark adaptation.

ERG responses recorded shortly after (5–10 min) and longer after (30–40 min) the conditioning flash are compared with responses from dark adapted mice in Figures 5A–5C. The changes in a_{max} and A that occur during dark adaptation are summarized in Figure 5D as fractions of their dark-adapted values. Both a_{max} and A completed

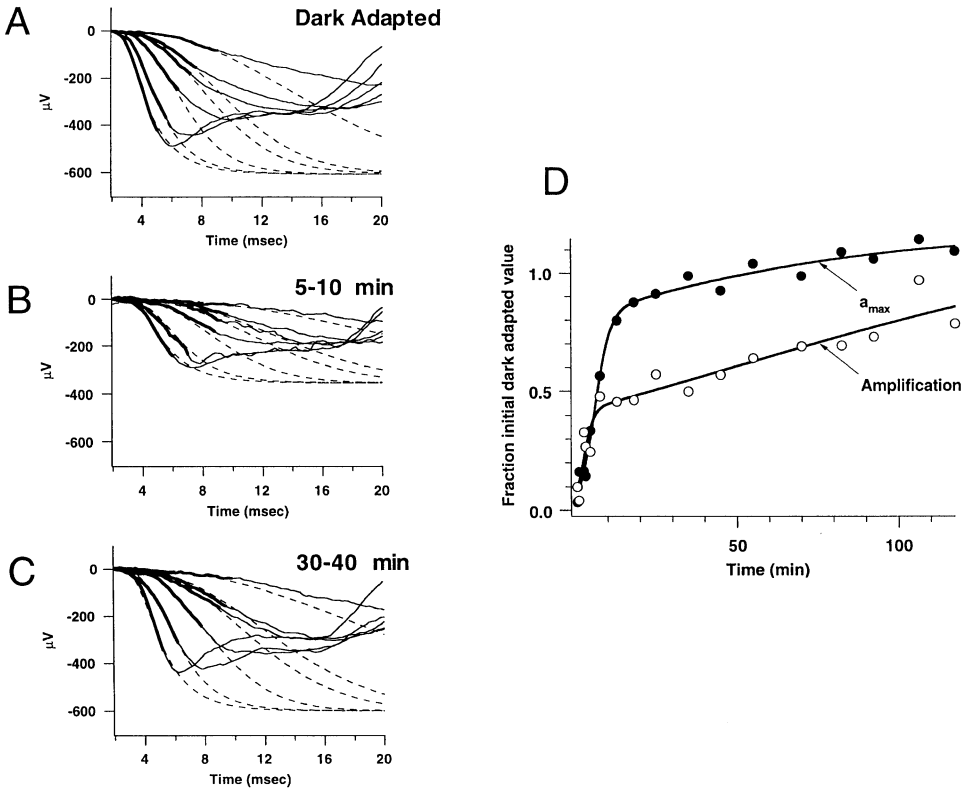

Figure 5. Recovery of ERG Parameters for Normal Mice Following a 20% Bleach

(A–C) ERG responses to flashes of dim to moderate intensity. The leading edges of the a-waves (shown in bold) were fit as an ensemble to a model of phototransduction as described in the Experimental Procedures. The fits are shown as dashed lines. Response families shown are from dark adapted mice (A), 5–10 min following a conditioning flash that bleached 20% of rhodopsin (B), and 30–40 min following the conditioning flash (C).

(D) Kinetics of recovery of a_{max} (closed circles) and the amplification factor, A (open circles), following the conditioning flash. All values for a_{max} and A were determined from the types of fits illustrated in (A)–(C). The solid lines were obtained by fitting the data to Equation 3.

an initial phase of recovery within ~10 min, but recoveries of both parameters were biphasic.

A theoretical framework for analyzing the time course of dark adaptation by electroretinography has been established (Thomas and Lamb, 1999). Residual transduction following conditioning illumination can be considered equivalent to fading background illumination. Using this analogy, the behavior of a_{max} during dark adaptation can be described by Equation 1:

$$a_{max}(t) = a_{max}(\infty)/[1 + c_a\exp(-k_a t)], \quad (1)$$

where $a_{max}(\infty)$ is the final dark adapted value, c_a specifies the degree of a_{max} reduction immediately after the bleach, T is time after the bleach, and k_a is the rate constant for recovery. The effect of either real background or equivalent background on a_{max} has been reported to fit a Michaelis-Menten type of saturation function:

$$a_{max}(I_B)/a_{max}(0) = I_0/(I_0 + I_B), \quad (2)$$

where $a_{max}(0)$ is the value in the absence of background illumination, I_B is the intensity of background illumination, and I_0 is the background intensity that reduces a_{max} by 50%. The equivalent background effect described by Equation 1 was derived from Equation 2 by considering lingering activity of the transduction mechanism as equivalent background illumination (Jones et al., 1996) and by including a factor to account for exponential decay of the equivalent background during dark adaptation (Thomas and Lamb, 1999). Since the first phase of recovery in our study was obviously much faster than the second, the following equation can be used as an approximation to fit the data in Figure 5D:

$$a_{max}(t) = a_{max}(\infty)/[1 + c_{a1}\exp(-k_{a1}t) + c_{a2}\exp(-k_{a2}t)], \quad (3)$$

where 1 and 2 refer to two different forms of equivalent background that have very different gain and very different decay rates. Equation 3 was used to fit dark adaptation of both a_{max} and A. For a_{max}, k_{a1} was 0.42/min and k_{a2} was 0.018/min. For A, $k_{a1}$was 0.67/min and k_{a2} was 0.013/min. The validity of using Equation 3 as an approximation was confirmed with these values using rate equations evaluated by an iterative numerical method.

The absolute values of *ca1* and *ca2* may not be directly converted to transduction gain. But it is reasonable to hypothesize that the molecular species that generate equivalent background 1 are fully converted to the species that generate equivalent background 2. The ratio of *ca1* to *ca2* should then accurately report the relative efficiencies with which these forms generate equivalent

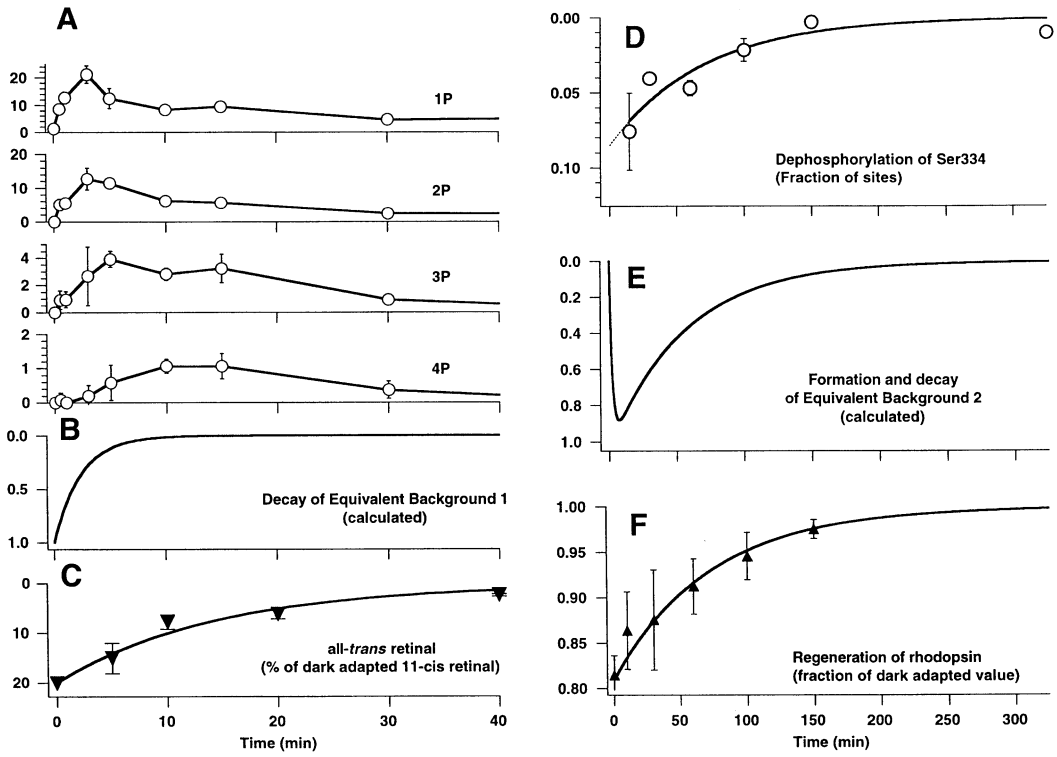

Figure 6. Comparisons of Reactions that Influence Deactivation of Phototransduction (A–C) and Recovery of Sensitivity (D–F)

(A) Kinetics of mono, double, triple, and quadruple phosphorylation following a conditioning flash that bleached 20% of rhodopsin. These are the data from Figure 3 presented on an expanded time scale. The y axis represents the percentage of total rhodopsin C termini in each phosphorylation state.

(B) The heavy solid line shows the calculated decay of equivalent background 1.

(C) Kinetics of reduction of all-*trans* retinal following the conditioning flash. The values are expressed as percentage of the dark adapted level of 11-*cis* retinal. The dark adapted level of all-*trans* retinal, 4%, was subtracted from all data points. The solid line is a single exponential fit of the data. The zero time point was calculated based on measurements of percentage of rhodopsin bleached.

(D) Dephosphorylation of Ser-334. The time course from Figure 3B is replotted. The solid line is a single exponential fit of the slow phase of dephosphorylation after 30 min. The dashed line is an extrapolation of that fit to zero time.

(E) The heavy solid line shows the formation (downslope) and then decay (upslope) of equivalent background 2 calculated from an iterative numerical solution of rate equations.

(F) Kinetics of rhodopsin regeneration following the conditioning flash. The solid line represents a single exponential fit of the data.

background in the transduction apparatus. The values of *ca1* and *ca2* were 16.3 and 0.47, respectively, for a_{max}, suggesting that the earlier sources are 35 times more efficient at stimulating transduction than later sources. The corresponding *ca1* and *ca2* values for *A* were 14.0 and 1.9, suggesting that the earlier sources are overall seven times more efficient at desensitizing transduction than the later sources.

The decay (0.42/min) of equivalent background 1 was calculated and is shown in Figure 6B. This rate is most similar to the rate at which the pool of photoactivated rhodopsin accumulates multiple phosphorylation. The sum of the initial rates of accumulation of double, triple, and quadruple phosphorylation was 0.35/min. This is much faster than reduction of all-*trans* retinal (0.07/min) (see below and Figure 6C). Conversion of the more active into the less active equivalent background, and the subsequent decay of equivalent background 2 are shown in Figure 6E. The curve is plotted with decay upward to facilitate comparison with panels D and F. Equivalent background 2 decays with the same time course as regeneration and dephosphorylation of rhodopsin.

Reduction of All-*trans* Retinal

To gain further insight into the chemistry underlying recovery of a_{max} and *A*, we measured reduction of all-*trans* retinal under the same conditions we used to measure phosphorylation and transduction parameters. All-*trans* retinal and opsin form a complex that stimulates transducin more efficiently than opsin alone (Sachs et al., 2000). The presence of this complex has been implicated as a long-lasting desensitizing product of phototransduction (Weng et al., 1999). We measured the rate of reduction of all-*trans* retinal under our standard conditions to be 0.07/min (Figure 6C and Table 2). This is slower than the decay of the "species 1" that generates the most active form of equivalent background. Therefore, reduction of all-*trans* retinal did not limit inactivation of phototransduction. However, reduction of retinal coincided with the transformation of opsin from predominantly a kinase substrate to a phosphatase substrate in agreement with the conclusions of a previous in vitro study (Hofmann et al., 1992). This suggests that one or more forms of all-*trans* retinal transiently maintained opsin in a form that stimulated rhodopsin kinase activity

Table 2. Kinetics[a] of Rhodopsin Regeneration, Reduction of All-*trans* Retinal, and Recovery of *A* and a_{max} Following a 20% Bleach

Rhodopsin regeneration	0.014/min
Reduction of all-*trans* retinal	0.07/min
Recovery of *A*	0.68/min, 0.013/min
Recovery of a_{max}	0.42/min, 0.018/min

[a] Rate constants were derived from single exponential fits to the experimental data for regeneration and reduction of retinal. The values reported for recovery of *A* and a_{max} refer to the rates of decay of two different forms of equivalent background as described in the text and determined by fitting the data shown in Figure 5D to Equation 3.

for the first 10–15 min following the conditioning flash. During that time, all-*trans* retinal was slowly reduced by all-*trans* retinal dehydrogenase. Subsequently, dephosphorylation predominated as rhodopsin kinase activity declined.

Phosphorylation and Dephosphorylation of Rhodopsin in CRALBP-Deficient Mice

To determine if dephosphorylation of rhodopsin depends on regeneration, we analyzed dephosphorylation in *Rlbp*$^{-/-}$ mice that do not express the CRALBP protein. Regeneration of rhodopsin is severely impaired in these mice because resynthesis of 11-*cis* retinal is delayed at the isomerisation step (Saari et al., 2001). We anaesthetized *Rlbp*$^{-/-}$ mice and normal mice, then exposed them to intense continuous illumination for 1.5 min. To most directly evaluate the effect of regeneration on dephosphorylation, we used an illumination protocol that bleached >99% of the rhodopsin in wild-type and *Rlbp*$^{-/-}$ retinas. We then quantitated phosphorylation of rhodopsin at various times out to 10 hr after bleaching. Phosphorylation and dephosphorylation were normal in the *Rlbp*$^{-/-}$ mice, except that some residual phosphorylation, mostly monophosphorylation, persisted in *Rlbp*$^{-/-}$ retinas (Figure 7A). We found that phosphorylation was increased above wild-type levels on all of the serine phosphorylation sites, Ser-343, Ser-338, and Ser-334 (data not shown).

The fraction of opsin that remained phosphorylated in fully bleached *Rlbp*$^{-/-}$ retinas was 0.2–0.3. This appeared to be similar to the estimated ratio of arrestin to rhodopsin (Langlois et al., 1996). Arrestin blocks dephosphorylation in vitro (Palczewski et al., 1989) and it binds phosphorylated opsin (Gurevich and Benovic, 1993), the species expected to be abundant at late times when regeneration is compromised by the *Rlbp*$^{-/-}$ mutation. Therefore, we performed an additional experiment to address the hypothesis that residual phosphorylation in *Rlbp*$^{-/-}$ mice arises from opsin-arrestin complexes that are refractory to dephosphorylation. Instead of bleaching 100% of rhodopsin, we bleached only 20%, an amount still in excess over arrestin. If tightly associated arrestin-opsin complexes are a source of phosphatase-resistant opsin, then the fraction of total opsin and rhodopsin phosphorylated following the 20% bleach should be the same as the fraction of opsin phosphorylated following 100% bleach.

Figure 7B shows that there was signficantly less persistent phosphorylation following 20% bleach than following 100% bleach. Furthermore, the levels of phosphorylation in normal and *Rlbp*$^{-/-}$ retinas were nearly indistinguishable after 20% bleach. These findings do not support the in vitro evidence that arrestin-opsin complexes inhibit dephosphorylation. More likely, the massive quantity of opsin that persists after the 100% bleach not only stimulates transducin, but also stimulates rhodopsin kinase activity in the fully bleached *Rlbp*$^{-/-}$ retinas.

Discussion

G protein-coupled receptors constitute a large class of topologically homologous proteins that sense environmental cues in the form of light, small molecules, Ca^{2+}, or polypeptide hormones. For rhodopsin and for many other G protein-coupled receptors, phosphorylation plays a critical role in terminating the coupling between the activated receptor and its cognate G protein. In order to reestablish sensitivity, the transduction cascade must be inactivated, the receptor must be dephosphorylated, and the agonist dissociated to return the receptor to its quiescent state. Many G protein-coupled receptors contain conserved serine/threonine phosphorylation sites near their C termini, implying that desensitization by phosphorylation is a general mechanism. Examples in addition to rhodopsin include the the β adrenergic receptor and the opioid receptor family; each is phosphorylated on its C termini in response to stimulation (Fredericks et al., 1996; Guo et al., 2000; Deng et al., 2000; Chen et al., 1995).

To enhance the general understanding of G protein-coupled receptor signaling dynamics and to resolve specific controversial issues about dark adaptation, we analyzed rod photoreceptor desensitization and subsequent resensitization following exposure to an intense light stimulus. We used two experimental approaches to evaluate rhodopsin phosphorylation. In our fast kinetics analysis, we used a novel rapid quench device to evaluate rates of phosphorylation in intact retinas immediately following an intense flash of light. This enabled us to establish the preferential order and initial rates of phosphorylation at each site on the rhodopsin C terminus. In our in vivo approach, we measured rates of several biochemical reactions under a specific set of conditions to directly evaluate their contributions to the physiology of recovery and dark adaptation. For these studies, we conditioned mouse eyes with an intense flash of light that bleached 20% of their rhodopsin. This condition was chosen because it allowed reliable measurement of rhodopsin phosphorylation, rhodopsin regeneration and all-*trans* retinal reduction using currently available methodology. In this report, we describe the development of these methods and how they reveal the underlying chemistry of recovery and adaptation. Future studies based on these methods will also address how multiple factors such as duration of light exposure and genetic deficiencies influence these reactions.

Kinetics and Site Specificity of Rhodopsin Phosphorylation

Previous studies reported that Ser-343 is the most favored phosphorylation site and that rhodopsin can be

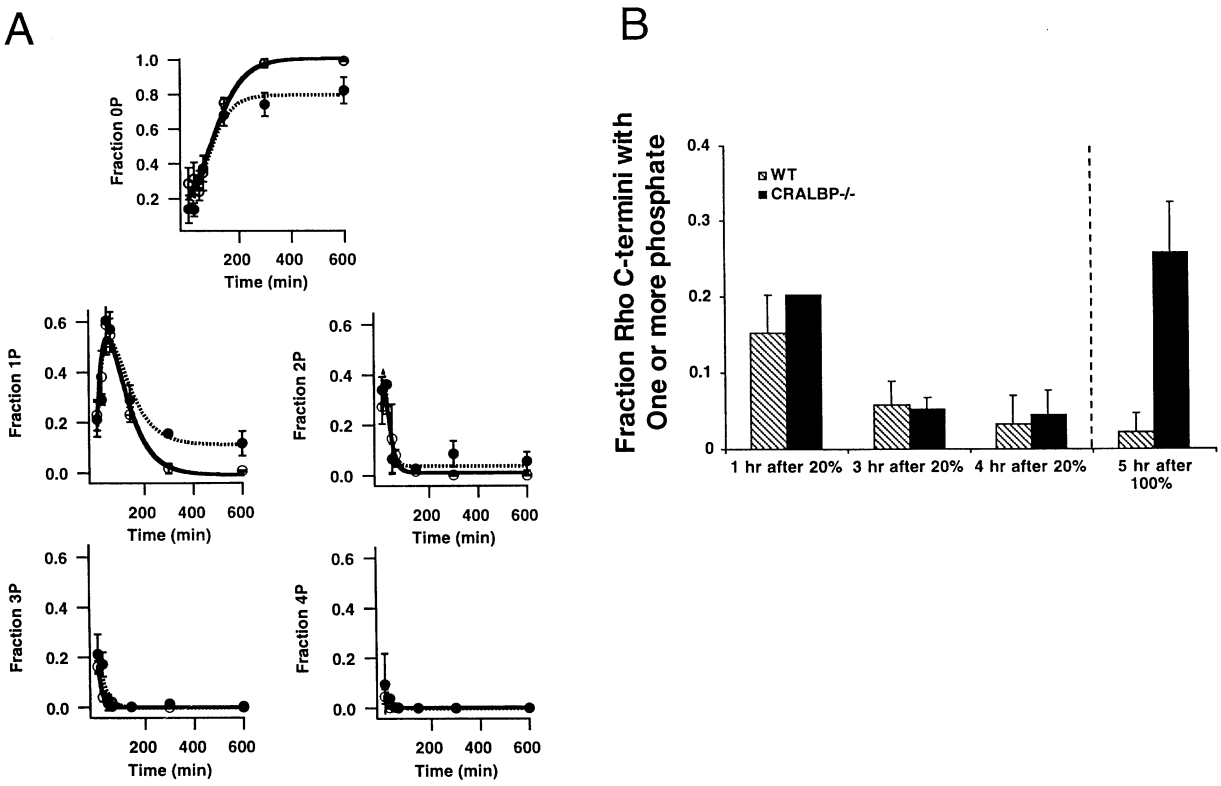

Figure 7. Rhodopsin Phosphorylation and Dephosphorylation in *Rlbp*$^{-/-}$ Mice

(A) Phosphorylation/dephosphorylation of *Rlbp*$^{-/-}$ mice (closed circles fit with dotted line) versus wild-type littermates (open circles fit with solid line) following continuous illumination for 1.5 min that bleached >99% of the rhodopsin.

(B) Levels of phosphorylation in wild-type (WT) and CRALBP-deficient mice 1, 3, and 4 hr following a flash of light bleaching 20% of the rhodopsin. These data are compared with phosphorylation levels in WT and CRALBP-deficient mice 5 hr after continuous illumination that bleached >99% of the rhodopsin (right side of vertical dotted line).

multiply phosphorylated in vitro (reviewed in Hurley et al., 1998). Evidence from a recent physiological study is also consistent with multiple phosphorylation of rhodopsin (Mendez et al., 2000). In contrast, the only previous in vivo study of rhodopsin phosphorylation (Ohguro et al. 1995) reported that Ser-338 rather than Ser-343 is the initial phosphorylation site and that multiple phosphorylation of rhodopsin does not occur in vivo. Our study agrees with the earlier findings that Ser-343 is the most favored site and that multiple phosphorylation does occur. Improvements in experimental design, sensitivity of detection, quenching efficiency, and time resolution may be responsible for the differences between our findings and the previous in vivo study. As further evidence for multiple phosphorylation, it should also be noted that an antibody that labels outer segments after bleaching (Ohguro et al., 1995) reportedly recognizes only multiply phosphorylated rhodopsins (Adamus et al., 1988).

Our study showed that initially sites closest to the C terminus of opsin are phosphorylated fastest. Ser-343 was phosphorylated most rapidly followed by Ser-338. Ser-334 was phosphorylated only after a delay of more than 10 s. Singly, doubly, and triply phosphorylated rhodopsins accumulated during the first few minutes following the flash. Low levels of quadruply phosphorylated peptides were also detected providing evidence for threonine phosphorylation.

It is not clear what determines the initial phosphorylation site preference. One possibility is that it is determined by a specific structure of the rhodopsin C terminus that causes Ser-343 to be better recognized by the kinase. An ordered structure of the rhodopsin C terminus has been proposed based on NMR analyses of model peptides (Yeagle et al., 1995). However, in a recently reported rhodopsin crystal structure (Palczewski et al., 2000), the last 15 amino acids of the C terminus, containing the phosphorylation sites, appear disordered. An alternative possibility is that the initial rates of phosphorylation may simply correlate with amino acid mobility and the frequency of collisions with the kinase. In support of this idea, a recent study described a gradient of mobility at the rhodopsin C terminus with the greatest mobility at the tip and the least near the membrane surface (Langen et al., 1999). Different initial rates of phosphorylation could also arise from steric or electrostatic interference near the membrane surface.

The delay before efficient Ser-334 phosphorylation began suggests several possible explanations:

(1) Phosphorylation at Ser-334 may be enhanced by prior phosphorylation at Ser-343 or Ser-338.
(2) Ser-334 may become more accessible independently of phosphorylation of the other sites as photoactivated rhodopsin makes its way through conformational transitions associated with bleaching.

(3) Ser-334 may be phosphorylated by a different kinase activated by molecular events stimulated by phototransduction (Greene et al., 1997).
(4) The sites might compete for rhodopsin kinase. At high bleach levels, rhodopsin kinase would be limiting. Under these conditions, the kinase may first phosphorylate all of the most favored C-terminal sites. Once that is completed, the kinase would turn its attention to Ser-334.

There is an important difference between these explanations. Hypotheses 1–3 predict that the delay could be the same following dim and bright flashes. But hypothesis 4 makes a different prediction. With a bright flash rhodopsin kinase would be limiting, but with a dim flash the kinase would be in excess over photoactivated rhodopsin. Therefore, hypothesis 4 predicts that a dimmer flash would reduce the delay before Ser-334 is modified. Further studies done over a range of flash intensities and using mice expressing mutant forms of rhodopsin will address these types of questions.

At the peak of phosphorylation in our 20% bleach experiments, ~35% of receptors had become phosphorylated, so some rhodopsin kinase must have been stimulated to phosphorylate unbleached rhodopsins. Only receptors modified at Ser-343 were produced in excess over the percentage bleached. Ser-343 was dephosphorylated rapidly after ~3 min, suggesting that phosphates on unbleached rhodopsin are rapidly removed. Multiple phosphorylation was achieved by only 16% ± 4% of the receptors. That is similar to percentage of rhodopsin bleached suggesting that only photoactivated molecules achieve multiple phosphorylation.

Dephosphorylation

Our measurements of rhodopsin dephosphorylation in vivo show that a phosphatase in rod outer segments effectively dephosphorylates the C-terminal sites. The time course of appearance and disappearance of quadruple phosphorylation (Figure 6A) shows that these sites are transformed from predominantly kinase substrates into predominantly phosphatase substrates between 10–15 min after the conditioning flash. This happened during the time that all-*trans* retinal was being reduced ($k = 0.07$/min or $\tau = 14$ min), suggesting that some step linked to the removal of all-*trans* retinal plays an important role in this transformation.

Dephosphorylation also proceeded in a preferential manner with Ser-343 being dephosphorylated the fastest, followed by Ser-338 and then Ser-334. The factors that influence order of dephosphorylation could be the same that influence phosphorylation, mobility differences, or steric factors.

Dark Adaptation and Electroretinography

An isolated photoreceptor has no access to the retinal pigment epithelium, the primary source of 11-*cis* retinal required for rhodopsin regeneration. Therefore, electrical recordings from isolated photoreceptors do not provide complete information about recovery and dark adaptation following extensive bleaching. Instead, electroretinography is the method of choice for this type of study. Quantitative methods that use ERG a-wave analysis to evaluate phototransduction have been established (Lyubarsky and Pugh, 1996; Hetling and Pepperberg, 1999; Lamb and Pugh, 1992; Thomas and Lamb, 1999). We used electroretinography to analyze phototransduction following a bright conditioning flash using a protocol identical to that used in our biochemical measurements.

Inactivation of Phototransduction

The recovery of a_{max} reflects reopening of cation channels, generally accepted as the "readout" of phototransduction inactivation in most physiological studies. When a large excess of photoactivated rhodopsin is produced, as in our experiments, the limiting step in photoresponse turnoff must be deactivation of rhodopsin. This simplified our analysis because rates of GTP hydrolysis and arrestin binding should not limit transduction inactivation in our experiments. It is this simplification that allowed us to directly compare rates of mono, double, or triple phosphorylation and the rate of reduction of all-*trans* retinal with photoresponse turnoff.

Figure 6 reports the physiological conclusions of our study. We evaluated inactivation of phototransduction using an equivalent background model of dark adaptation (Thomas and Lamb, 1999). Residual transduction lingering after the conditioning flash was considered equivalent to fading background illumination. The biphasic recoveries shown in Figure 5D and the good fit using Equation 3 suggest two classes of equivalent background that stimulate phototransduction with different efficiencies and decay at different rates. Figure 6B represents the most active (highest gain) equivalent background being quenched at rate of 0.42/min. We refer to this as "equivalent background 1." The recovery of a_{max} shown in Figure 5D appears slower than this because rods remain in saturation during most of the initial decay of equivalent background 1.

Quenching of "Equivalent Background 2"

Inactivation of equivalent background 2 caused the slow phase of recovery of amplification and a_{max}. Figures 6D–6F compare regeneration and dephosphorylation kinetics with the formation and decay of equivalent background 2. The production of equivalent background 2 from equivalent background 1 (downslope) and the subsequent inactivation of equivalent background 2 (upslope) are shown in Figure 6E. Equivalent background 2 was quenched at the same rate as rhodopsin was regenerated (Figure 6F).

Molecular Origins of Equivalent Background Light during Dark Adaptation

Equivalent background 1 decayed at a rate of 0.42/min, about the same rate as accumulation of multiple phosphorylation (0.35/min) and faster than reduction of all-*trans* retinal (0.07/min). Metarhodopsin II decays at a rate of 0.47/min based on spectrophotometric measurements using rat rods (Catt et al., 1982). Therefore, equivalent background 1 decay most likely consists of several molecular components including decay of metarhodopsin II, phosphorylation of metarhodopsin II, decay of phosphorylated metarhodopsin II, phosphorylation of opsin/all-*trans* retinal complexes, and perhaps transport

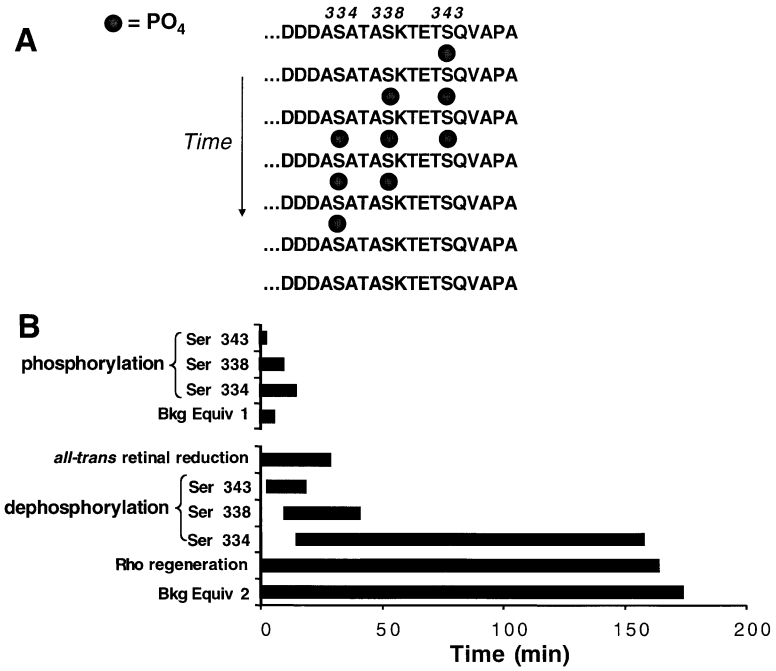

Figure 8. Models for Rhodopsin Phosphorylation

(A) Cartoon summarizing the kinetic analyses of rhodopsin phosphorylation. Phosphorylation and dephosphorylation occur most rapidly at Ser-343 closest to the C terminus.

(B) A chronology of the events occurring during dark adaptation following an intense conditioning flash. The filled bars represent the time for each reaction to proceed to 90% completion following the conditioning flash. Opsin dephosphorylation became predominant after a short delay represented by the open bars at early times.

of all-trans retinal from disks (Weng et al., 1999). Equation 3 is therefore only an approximation that summarizes the overall gain and overall decay of the various species that contribute to equivalent background 1.

The slowly fading equivalent background 2 also appears to originate in multiple molecular species. It was initially formed as multiple phosphorylation was accumulating and before most of the all-*trans* retinal had been reduced. Therefore, the first molecular origin of this equivalent background was most likely either phosphorylated metarhodopsin II or phosphorylated opsin bound to all-*trans* retinal. However, equivalent background 2 decayed at an overall rate of ~0.016/min, which is much slower than the 0.07/min rate of reduction of all-*trans* retinal produced by the conditioning flash. Therefore, equivalent background 2 during the later stages of dark adaptation must have arisen from species that do not contain all-*trans* retinal. As confirmation of this, we noted that dephosphorylation began to overwhelm phosphorylation while all-*trans* retinal was being reduced. This indicated that a molecular transformation in opsin was taking place. In summary, phosphorylated metarhodopsin II that contributed to equivalent background during the first ~20 min (Leibrock et al., 1998) could not have contributed significantly to the slowly fading equivalent background 2 after that. Residual transduction stimulated by opsin is known to cause desensitization (Melia et al., 1997; Fain et al., 1996). So the most likely source of equivalent background 2 after 20 min was opsin and/or opsin monophosphorylated primarily at Ser-334.

According to our analysis, the overall gain of equivalent background 1 was ~35 times higher than the gain of equivalent background 2. For comparison, the ratio of metarhodopsin II to opsin transduction activity is $\sim 10^5$ (Melia et al., 1997, Cornwall and Fain, 1994), whereas the ratio of all-*trans* retinal/opsin to opsin activity is ~10 (Jager et al., 1996).

Loss and Recovery of Sensitivity

The reduction of amplification and its biphasic recovery shown in Figure 5D were calculated from the a-wave fitting protocol. Changes in quantum catch caused by bleaching and regeneration of rhodopsin were corrected for in the analysis using our direct measurements of rhodopsin regeneration (Figure 6F). The biphasic recovery of amplification was also analyzed with the equivalent background model (Thomas and Lamb, 1999). The rapid phase of amplification recovery (0.67/min) was similar to the rapid recovery of a_{max} (0.42/min) attributable to inactivation of metarhodopsin II or opsin/all-*trans* retinal complexes. Based on this analysis, we estimate that equivalent background 1 is seven times more effective at reducing gain than "equivalent background 2," the less active and slower decaying species. This is less than the corresponding ratio, 35×, for the efficiencies with which equivalent background 1 and 2 stimulate transduction. The values of *ca1* and *ca2* derived from Equation 3 suggest that there is a more pronounced effect of equivalent background 2 on gain reduction than on transduction stimulation in comparison to the effects of equivalent background 1.

Comparison with Human Dark Adaptation Studies

The rate of decay of equivalent background 1 is consistent with a previous report that described dark adaptation of human subjects measured by electroretinography (Thomas and Lamb, 1999). Following a full bleach, the equivalent background in that study decayed at a rate of 0.35/min. In our study, in which 20% of rhodopsin was bleached in a mouse eye, equivalent background 1 decayed at a rate of 0.42/min. The slower decaying form of equivalent background was not detected in the human study, suggesting substantial differences in regeneration kinetics between humans and mice. Our value for the decay of equivalent background 1 also

approximates the kinetics of visual threshold recovery in psychophysical experiments (k = 0.56/min) (Lamb, 1981).

Another important difference between our findings and those of the human study is that photobleaching reduced the amplification constant in mice but not in humans (Thomas and Lamb, 1999). There was an apparent reduction in that parameter in humans, but it was attributed entirely to reduced quantum catch resulting from loss of rhodopsin. In our study, we directly measured the amount of rhodopsin present during dark adaptation and we corrected for the loss in quantum catch in our calculations. But even with that correction, the amplification factors we determined were significantly reduced (Figure 5D). The slow recovery of amplification during dark adaptation matched the kinetics of rhodopsin regeneration and dephosphorylation, suggesting that the presence of opsin or phosphorylated opsin actively reduces the gain of phototransduction. The difference between our study and the human study may reflect the species difference, the differences in the type of conditioning illumination (one brief flash in our study versus steady illumination or several brief flashes in the human study), or the use of anesthetic with mice but not with humans.

Origin of Residual Rhodopsin Phosphorylation in Bleached *Rlbp*$^{-/-}$ Retinas

We investigated the relationship between dephosphorylation and regeneration of rhodopsin by comparing phosphorylation in normal and in regeneration deficient retinas. Following an ~100% bleach, the initial rate of dephosphorylation was unaffected by the blocked regeneration. However, we discovered that a fraction of the opsin pool in *Rlbp*$^{-/-}$ retinas was persistently phosphorylated. An obvious hypothesis consistent with this observation is that binding of arrestin to opsin interferes with dephosphorylation. However, the results of a separate set of experiments were not consistent with this hypothesis. A more likely explanation for the residual phosphorylation is that rhodopsin kinase is stimulated by the massive amounts of unregenerated opsin in the fully bleached *Rlbp*$^{-/-}$ retinas.

Concluding Remarks

A model that summarizes our analysis of phosphorylation and dephosphorylation of photoactivated rhodopsin in vivo is shown in Figure 8A. Figure 8B summarizes our results as a chronology of events that occur during recovery and dark adaptation following a conditioning flash.

The study we report here accurately and directly measured the kinetics and site specificity of rhodopsin phosphorylation and dephosphorylation in vivo during recovery from a photobleach. It directly compares the physiology of dark adaptation with the kinetics of the multiple fundamental chemical reactions that govern it. Integration of biochemical and physiological methodology as described in this report can now be used, along with further genetic manipulations, to resolve the molecular basis of photoreceptor turnoff and dark adaptation under a variety of illumination conditions.

Experimental Procedures

Rhodopsin Phosphorylation/Dephosphorylation

Rhodopsin phosphorylation was measured using a procedure substantially modified from Hurley et al. (1998). Mice were dark adapted overnight for all the experiments reported here. All manipulations at light-sensitive steps in the analysis were done under infrared illumination. For rapid time points, a mouse was sacrificed by cervical dislocation, eyes were removed, and retinas were quickly dissected into 50 μl of an oxygenated Locke's solution (140 mM NaCl, 0.6 mM KCl, 1.2 mM $CaCl_2$, 2.4 mM $MgCl_2$, 3 mM HEPES [pH 7.4], 10 mM glucose) at 37°C. The solution was transferred to the translucent sample tube of the apparatus shown in Figure 1. Flashes were delivered unattenuated from a Canon 540EZ Speedlite flash unit focused onto the bottom of the tube through a fiber optic cable and lens. At specific times from 125 ms to 60 s after the flash, the computer activated a solenoid valve to open for 1 s to allow 700 μl of 7 M deionized urea, 5 mM EDTA, 20 mM Tris (pH 7.4) to flow into the tube. Simultaneously, a solenoid was activated to push the tube for 1 s onto the tip of a homogenizer (Ultra-Turrax) rotating at 20,000 rpm. The membranes were then harvested by centrifugation at 54,000 rpm in a Beckman TLA-55 rotor in a tabletop Beckman Optima ultracentrifuge. The membranes were washed twice with deionized water, resuspended in 25 μl of 20 μg/ml Asp-N protease (Roche, Indianapolis) in 10 mM HEPES (pH 7.4), and incubated at room temperature for 17 hr. The solubilized peptides were then recovered in the supernatant after centrifugation at 54,000 rpm. The supernatants were diluted to 90 μl, acidified with 10 μl of 5% acetic acid, and stored at −20°C.

For in vivo experiments, mice were dark adapted overnight, anaesthetized with a xylazine/ketamine mix, and one eye was exposed to the flash from the fiber optic in the same configuration used for ERG measurements. At the specified time, the mouse was sacrificed by cervical dislocation, and the eye was removed and immediately homogenized in the apparatus shown in Figure 1. The samples were then treated as described in the preceding paragraph.

Samples were typically analyzed by using a Perkin-Elmer autosampler to inject 20 μl onto a 260 μm × ~5 cm capillary column (packed with Vydac C18 resin at ~1000 psi) at a flow rate of 2–4 μl/min. Samples were loaded in 0.08% heptafluorobutyric acid (HFBA) (Ohguro et al., 1995) and typically eluted isocratically in 0.08% HFBA, 20% acetonitrile. The exact percent acetonitrile used for a set of analyses varied depending on the column size and flow rates used. The elution order of the phosphorylated peptides was invariant but elution times of the phosphorylated species varied. Elution times and the identity of each peak in each experiment were established using CID ions characteristic of each species. The cycle time for each analysis was 65 min, including time to wash and reequilibrate the column. The eluate was sprayed through a 15 μm needle (New Objective, Cambridge, MA) into a Finnigan LCQ deca ion trap mass spectrometer with automatic gain control off. Ions were detected in positive ion mode with an injection time of 20 ms. Recovery of C-terminal peptides from the entire intact retina procedure was estimated to be 10%–30% starting with 1 nmol of rhodopsin from two eyes and based on calibrations using synthetic peptide standard solutions quantitated by amino acid analysis. Recoveries from the whole eye homogenates were generally higher. We reanalyzed several samples at different concentrations and found the results to be independent of concentration at least 2-fold over and under the range typically used in our experiments. CID analyses of mono- and doubly phosphorylated species were performed using an activation amplitude of 20.5%, activation Q of 0.250, activation time of 50 ms, and isolation width of 2.5 m/z.

Synthetic peptides were used as standards to determine elution positions, for optimization of the CID methods and for quantitating the effect of phosphorylation on efficiency of detection. They were prepared by Anaspec (San Jose, CA) with phosphoserines either at the 334, 338, or 343 positions and were quantitated in duplicate by amino acid analysis (AAA Laboratories, Mercer Island, WA). The three different monophosphorylated peptides were detected with equal efficiencies with the ion trap. To estimate the effects of phosphorylation on efficiency of peptide detection, we used standards of unphosphorylated, mono-, double-, triple-, quadruple-, and quintuple-phosphorylated bovine rhodopsin C-terminal peptides cleaved and

purified from heavily phosphorylated bovine ROS. The peptides were quantitated by amino acid analysis, and the reductions in efficiency of detection caused by phosphorylation state were analyzed using the same type of chromatography and mass spectrometry analyses used to analyze experimental samples. We also determined the reduction in detection efficiency caused by monophosphorylation of the corresponding mouse peptide. We then used the relationship between phosphorylation and detection efficiency established from the bovine peptide analysis to calculate the corresponding efficiencies for detecting mouse peptides in their various phosphorylation states. Based on this analysis, we calculated fractions of mono-, double-, triple- and quadruple-phosphorylated mouse peptides in our experimental samples using the following factors to correct for loss of detection efficiency with increasing level of phosphorylation: unphosphorylated, 1; monophosphorylated, 1.35; doubly phosphorylated, 1.54; triply phosphorylated, 1.69; quadruply phosphorylated, 1.82. Quantitation of each species was calculated as a fraction of the total peptides detected. For example, the fraction of peptides in the monophosphorylated state is:

$$(1.35*\mathrm{Area}_{973})/[\mathrm{Area}_{933} + (1.35*\mathrm{Area}_{973}) + (1.54*\mathrm{Area}_{1013}) + (1.69*\mathrm{Area}_{1053}) + (1.82*\mathrm{Area}_{1093})].$$

Rhodopsin Regeneration

Rhodopsin regeneration was measured following a previously developed protocol (Van Hooser et al., 2000). Briefly, mice were sacrificed by cervical dislocation at various times following a flash bleaching 20% of the rhodopsin. All operations were performed under infrared illumination. Eyes (three to four per analysis) were dissected, rinsed, and collected in a 1.5 ml microfuge tube on dry ice and stored at −80°C until analysis. The eyes were homogenized in 0.5 ml of 20 mM BTP (Bis-Tris Propane, 1,3-bis[tris{hydroxymethyl}amino]propane) [pH 7.5] containing 10 mM dodecyl-β-maltoside and 5 mM hydroxylamine. The samples were vortexed vigorously and shaken at room temperature for 10 min. The homogenate was centrifuged at 14,000 rpm for 5 min at room temperature, and the supernatant was saved. The pellet was reextracted following the above procedure. Absorption spectra were obtained before and after bleaching (4 min at 1 mW/cm^2). The difference in absorbance at 500 nm was used to calculate the concentration of rhodopsin (ϵ = 42,000 M^{-1}cm^{-1}).

Retinoid Analysis

Mouse eyes were collected as for rhodopsin regeneration experiments. Retinoids were extracted from thawed, whole mouse eyes (four per analysis) using 10 mM hydroxylamine and analyzed with a normal phase HPLC column as previously described (Garwin and Saari, 2000).

Electroretinography

Mice were dark adapted for at least 15 hr and anaesthetized with intraperitoneal injection of Ketamine and Xylazine (140 mg/kg and 0.5 mg/kg body weight, respectively). Pupils were dilated by topical application of tropicamide and phenylephrine 15–20 min before any ERGs were recorded. Mice were placed on a glass manifold connected to a circulating water bath held at 37°C. All manipulations were done under infrared illumination. Flashes were delivered from a photographic flash unit focused on the eye through a fiber optic cable and lens. A gold ring electrode embedded in a contact lens (Bayer et al., 2000) was placed on a drop of 2%–3% methyl cellulose on the cornea and a copper reference electrode was placed in the mouth. The unattenuated energy of the flash measured at the position of the cornea was 2.9 mJ/cm^2. This intensity was used for the light-adapting flash for intact retinas and for in vivo experiments. ERG signals were amplified 10,000×, filtered between 1 Hz to 3 kHz, and sampled at 5 kHz. Data were collected and analyzed with Igor Pro using a suite of data acquisition software developed by Fred Rieke (Dept. of Physiology and Biophysics, University of Washington). Responses to test flashes from dim to moderate intensity caused 1600, 5900, 8700, 22300, 92700, and 292,000 photoisomerisations per rod in dark adapted wild-type mice based on comparisons with the amplification factor determined from mouse ERGs calibrated by Lyubarsky and Pugh (1996). These values were also consistent with the time of the a-wave peak amplitude for these flash responses.

For dark adaptation experiments, responses to two to three different test flash intensities were collected from each mouse at various times following a conditioning flash of light that bleached 20% of rhodopsin. When the brightest flashes were used, they were applied at intervals of 4–5 min or longer to avoid perturbing dark adaptation. Dark adaptation experiments were performed in this manner using 18 mice. Each trace shown in Figure 5A represents an average of 15 recordings, in Figure 5B 4–11 recordings were averaged per trace and in Figure 5C 12–22 were averaged. These were representative of all the data shown in Figure 5D. The analyses of the leading edge of the a-waves were based on the Lamb and Pugh model for activation of the phototransduction cascade:

$$a = a_{max}\,(1 - \exp[0.5A\phi(t - t_d)^2]), \quad (4)$$

where a is the a-wave amplitude at time t, a_{max} is the maximum a-wave amplitude that would be produced in the absence of synaptic transmission to bipolar cells, A is a factor proportional to the gain of phototransduction, ϕ is the number of photoisomerisations per rod, and t_d is an intrinsic delay time. The a-waves from all flash intensities were fit simultaneously using a variation of this equation (Smith and Lamb, 1997) that takes into account the capacitative time constant (τ) of the photoreceptor. Fitting was performed using the Global Fit program of Igor Pro (Wavemetrics). The portions of the a-wave used for fitting are shown as thicker traces in Figures 5A–5C. The values of τ and t_d were kept constant for fitting each family but were varied within a narrow range during the time course of dark adaptation. The optimal values of τ ranged from 1.8 ms at the beginning of dark adaptation to 1.4 ms after about 50 min and t_d varied randomly from 1.9 –2.5 ms. Fitting of responses recorded during dark adaptation was accomplished by linearly correcting the dark adapted values of ϕ based on the reduced amount of rhodopsin present at each time. The correction factor for ϕ used was the relative fraction of rhodopsin present at the time of the test flash compared to the dark adapted level. These values were determined from the regeneration data in Figure 6D. Cone contributions to the a-wave responses were considered to be negligible except perhaps during the first ~2 min after the conditioning flash. A small correction was applied to account for a 25 μV contribution of cones to a_{max} throughout the dark adaptation period, but the effects of this adjustment on any of the parameters were negligible.

Acknowledgments

We thank Fred Rieke for computer software and advice, Rick Newitt and Lowell Erickson for advice on mass spectrometry, Maria Nawrot for assistance with *Rlbp*$^{-/-}$ knockout mice, and Susan Brockerhoff, Peter Detwiler, and Bertil Hille for critical reading of sections of the manuscript. These studies were supported by the Howard Hughes Medical Institute, grants EY06641 (J.B.H.), and EY02317 (J.C.S.) from the National Eye Institute, the University of Washington Molecular and Cellular Biology Training Grant 5T32 GM07270 (M.J.K.), and an unrestricted grant to the University of Washington Department of Ophthalmology from Research to Prevent Blindness, Inc. (RBP). J.C.S. is a senior scientific investigator of RBP.

Received October 5, 2000; revised April 25, 2001.

References

Adamus, G., Zam, Z.S., McDowell, J.H., Shaw, G.P., and Hargrave, P.A. (1988). A monoclonal antibody specific for the phosphorylated epitope of rhodopsin comparison with other anti-phosphoprotein antibodies. Hybridoma *7*, 237–247.

Bayer, A.U., Mittag, T., Cook, P., Brodie, S.E., Podos, S.M., and Maag, K.P. (2000). Comparisons of the amplitude size and the reproducibility of three different electrodes to record the corneal flash electroretinogram in rodents. Doc. Ophthal. *98*, 233–246.

Breton, M.E., Schueller, A.W., Lamb, T.D., and Pugh, E.N., Jr. (1994). Analysis of ERG a-wave amplification and kinetics in terms of the

G-protein cascade of phototransduction. Invest. Ophthamol. Vis. Sci. *35*, 295–309.

Catt, M., Ernst, W., and Kemp, C.M. (1982). The links between rhodopsin bleaching and visual adaptation. Biochem. Soc. Trans. *10*, 343–345.

Chen, J., Makino, C.L., Peachey, N.S., Baylor, D.A., and Simon, M.I. (1995). Mechanisms of rhodopsin inactivation in vivo as revealed by a COOH-terminal truncation mutant. Science *267*, 374–377.

Cornwall, M.C., and Fain, G.L. (1994). Bleached pigment activates transduction in isolated rods of the salamander retina. J. Physiol. (Lond.) *480*, 261–79.

Deng, H.B., Yu, Y., Pak, Y., O'Dowd, B.F., George, S.R., Surratt, C.K., Uhl, G.R., and Wang, J.B. (2000). Role for the C-terminus in agonist-induced mu opioid receptor phosphorylation and desensitization. Biochemistry *39*, 5492–5499.

Fain, G.L., Matthews, H.R., and Cornwall, M.C. (1996). Dark adaptation in vertebrate photoreceptors. Trends Neurosci. *19*, 502–507.

Fain, G.L., Matthews, H.R., Cornwall, M.C., and Koutalos, Y. (2001). Adaptation in vertebrate photoreceptors. Physiol. Rev. *81*, 117–151.

Fredericks, Z.L., Pitcher, J.A., and Lefkowitz, R.J. (1996). Identification of the G protein-coupled receptor kinase phosphorylation sites in the human beta2-adrenergic receptor. J. Biol. Chem. *271*, 13796–13803.

Fuchs, S., Nakazawa, M., Maw, M., Tamai, M., Oguchi, Y., and Gal, A. (1995). A homozygous 1-base pair deletion in the arrestin gene is a frequent cause of Oguchi disease in Japanese. Nat. Genet. *10*, 360–362.

Garwin, G.G., and Saari, J.C. (2000). High-performance liquid chromatography analysis of visual cycle retinoids. Meth. Enzymol. *316*, 313–324.

Greene, N.M., Williams, D.S., and Newton, A.C. (1997). Identification of protein kinase C phosphorylation sites on bovine rhodopsin. J. Biol. Chem. *272*, 10341–10344.

Guo, J., Wu, Y., Zhang, W., Zhao, J., Devi, L.A., Pei, G., and Ma, L. (2000). Identification of G protein-coupled receptor kinase 2 phosphorylation sites responsible for agonist-stimulated delta-opioid receptor phosphorylation. Mol. Pharmacol. *58*, 1050–1056.

Gurevich, V.V., and Benovic, J.L. (1993). Visual arrestin interaction with rhodopsin. Sequential multisite binding ensures strict selectivity toward light-activated phosphorylated rhodopsin. J. Biol. Chem. *268*, 11628–11638.

Hetling, J.R., and Pepperberg, D.R. (1999). Sensitivity and kinetics of mouse rod flash responses determined in vivo from paired-flash electroretinograms. J. Physiol. (Lond.) *516*, 593–609.

Hofmann, K.P., Pulvermuller, A., Buczylko, J., Van Hooser, P., and Palczewski, K. (1992). The role of arrestin and retinoids in the regeneration pathway of rhodopsin. J. Biol. Chem. *267*, 15701–15706.

Hurley, J.B., Spencer, M., and Niemi, G.A. (1998). Rhodopsin phosphorylation and its role in photoreceptor function. Vis. Res. *38*, 1341–1352.

Jager, S., Palczewski, K., and Hofmann, K.P. (1996). Opsin/all-trans-retinal complex activates transducin by different mechanisms than photolyzed rhodopsin. Biochemistry *35*, 2901–2908.

Jones, G.J., Cornwall, M.C., and Fain, G.L. (1996). Equivalence of background and bleaching desensitization in isolated rod photoreceptors of the larval tiger salamander. J. Gen. Physiol. *108*, 333–340.

Lamb, T.D. (1981). The involvement of rod photoreceptors in dark adaptation. Vision Res. *21*, 1773–1782.

Lamb, T.D., and Pugh, E.N., Jr. (1992). A quantitative account of the activation steps involved in phototransduction in amphibian photoreceptors. J. Physiol. *449*, 719–758.

Langen, R., Cai, K., Altenbach, C., Khorana, H.G., and Hubbell, W.L. (1999). Structural features of the C-terminal domain of bovine rhodopsin: a site-directed spin-labeling study. Biochemistry *38*, 7918–7924.

Langlois, G., Chen, C.K., Palczewski, K., Hurley, J.B., and Vuong, T.M. (1996). Responses of the phototransduction cascade to dim light. Proc. Natl. Acad. Sci. USA *93*, 4677–4682.

Leibrock, C.S., Reuter, T., and Lamb, T.D. (1998). Molecular basis of dark adaptation in rod photoreceptors. Eye *12*, 511–520.

Lyubarsky, A.L., and Pugh, E.N., Jr. (1996). Recovery phase of the murine rod photoresponse reconstructed from electroretinographic recordings. J. Neurosci. *16*, 563–571.

McDowell, J.H., Nawrocki, J.P., and Hargrave, P.A. (1993). Phosphorylation sites in bovine rhodopsin. Biochemistry *32*, 4968–4974.

Melia, T.J., Jr., Cowan, C.W., Angleson, J.K., and Wensel, T.G. (1997). A comparison of the efficiency of G protein activation by ligand-free and light-activated forms of rhodopsin. Biophys. J. *73*, 3182–3191.

Mendez, A., Burns, M.E., Roca, A., Lem, J., Wu, L.W., Simon, M.I., Baylor, D.A., and Chen, J. (2000). Rapid and reproducible deactivation of rhodopsin requires multiple phosphorylation sites. Neuron *28*, 153–164.

Ohguro, H., Palczewski, K., Ericsson, L.H., Walsh, K.A., and Johnson, R.S. (1993). Sequential phosphorylation of rhodopsin at multiple sites. Biochemistry *32*, 5718–5724.

Ohguro, H., Van Hooser, J.P., Milam, A.H., and Palczewski, K. (1995). Rhodopsin phosphorylation and dephosphorylation *in vivo*. J. Biol. Chem. *270*, 14259–14262.

Palczewski, K., McDowell, J.H., Jakes, S., Ingebritsen, T.S., and Hargrave, P.A. (1989). Regulation of rhodopsin dephosphorylation by arrestin. J. Biol. Chem. *264*, 15770–15773.

Palczewski, K., Kumasaka, T., Hori, T., Behnke, C.A., Motoshima, H., Fox, B.A., Le Trong, I., Teller, D.C., Okada, T., Stenkamp, R.E., et al. (2000). Crystal structure of rhodopsin: a G protein-coupled receptor. Science *289*, 739–745.

Papac, D.I., Oatis, J.E., Jr., Crouch, R.K., and Knapp, D.R. (1993). Mass spectrometric identification of phosphorylation sites in bleached bovine rhodopsin. Biochemistry *32*, 5930–5934.

Saari, J.C., Nawrot, M., Kennedy, B.N., Garwin, G.G., Hurley, J.B., Huang, J., Possin, D.E., and Crabb, J.W. (2001). Visual cycle impairment in cellular retinaldehyde binding protein (CRALBP) knockout mice results in delayed dark adaptation. Neuron *29*, 739–748.

Sachs, K., Maretzki, D., Meyer, C.K., and Hofmann, K.P. (2000). Diffusible ligand all-trans-retinal activates opsin via a palmitoylation-dependent mechanism. J. Biol. Chem. *275*, 6189–6194.

Smith, N.P., and Lamb, T.D. (1997). The a-wave of the human electroretinogram recorded with a minimally invasive technique. Vision Res. *37*, 2943–2952.

Stecher, H., Gelb, M.H., Saari, J.C., and Palczewski, K. (1999). Preferential release of 11-cis-retinol from retinal pigment epithelial cells in the presence of cellular retinaldehyde-binding protein. J. Biol. Chem. *274*, 8577–8585.

Stiles, W.S., and Crawford, B.H. (1932). *Equivalent adaptational levels in localized retinal areas.* In Report of a Joint Discussion of Vision, Physical Society of London (Cambridge, UK: Cambridge University Press), pp. 194–211.

Thomas, M.M., and Lamb, T.D. (1999). Light adaptation and dark adaptation of human rod photoreceptors measured from the a-wave of the electroretinogram. J. Physiol. *518*, 479–496.

Van Hooser, J.P., Garwin, G.G., and Saari, J.C. (2000). Analysis of visual cycle in normal and transgenic mice. Meth. Enzymol. *316*, 565–575.

Weng, J., Mata, N.L., Azarian, S.M., Tzekov, R.T., Birch, D.G., and Travis, G.H. (1999). Insights into the function of Rim protein in photoreceptors and etiology of Stargardt's disease from the phenotype in ABCR knockout mice. Cell *98*, 13–23.

Winston, A., and Rando, R.R. (1998). Regulation of isomerohydrolase activity in the visual cycle. Biochemistry *37*, 2044–2050.

Xu, J., Dodd, R.L., Makino, C., Simon, M.I., Baylor, D.A., and Chen, J. (1997). Prolonged photoresponses in transgenic mouse rods lacking arrestin. Nature *389*, 505–509.

Yamamoto, S., Sippel, K.C., Berson, E.L., and Dryja, T.P. (1997). Defects in the rhodopsin kinase gene in the Oguchi form of stationary night blindness. Nat. Genet. *15*, 175–178.

Yamamoto, H., Simon, A., Eriksson, U., Harris, E., Berson, E.L., and Dryja, T.P. (1999). Mutations in the gene encoding 11-cis retinol dehydrogenase cause delayed dark adaptation and fundus albipunctatus. Nat. Genet. *22*, 188–191.

Yeagle, P.L., Alderfer, J.L., and Albert, A.D. (1995). Structure of the carboxy-terminal domain of bovine rhodopsin. Nat. Struct. Biol. *2*, 832–834.